# Transition strengths in the neutron-rich $^{73,74,75}$Ni isotopes

A. Gottardo,[1,2,*] G. de Angelis,[1] P. Doornenbal,[3] L. Coraggio,[4] A. Gargano,[4] N. Itaco,[4,5] K. Kaneko,[6] P. Van Isacker,[7] T. Furumoto,[8,3] G. Benzoni,[9] J. Lee,[3] H. Liu,[3] M. Matsushita,[10] D. Mengoni,[2] V. Modamio-Hoybjor,[1] S. Momiyama,[11] T. Motobayashi,[3] D. R. Napoli,[1] M. Niikura,[11] E. Sahin,[12] Y. Shiga,[3,13] H. Sakurai,[3,11] R. Taniuchi,[11] S. Takeuchi,[3] H. Wang,[3,14] J. J. Valiente-Dobòn,[1] R. Avigo,[9,15] H. Baba,[3] N. Blasi,[9] F. L. Bello Garrote,[12] F. Browne,[3,16] F. C. L. Crespi,[9,15] S. Ceruti,[9,15] R. Daido,[14] M.-C. Delattre,[17] D. Fang,[14] Zs. Dombradi,[18] T. Isobe,[3] I. Kuti,[18] G. Lorusso,[3] K. Matsui,[11] B. Melon,[19] T. Miyazaki,[11] S. Nishimura,[3] R. Orlandi,[20] Z. Patel,[3,21] S. Rice,[3,21] L. Sinclair,[3,22] P. A. Söderström,[3] D. Sohler,[18] T. Sumikama,[23] J. Taprogge,[24,25] Zs. Vajta,[18] H. Watanabe,[3,26] O. Wieland,[9] J. Wu,[3,23] Z. Y. Xu,[11] M. Yalcinkaya,[27] and R. Yokoyama[10]

[1]*Istituto Nazionale di Fisica Nucleare, Laboratori Nazionali di Legnaro, Legnaro I-35020, Italy*
[2]*Dipartimento di Fisica e Astronomia dell'Università degli Studi di Padova, Padova I-35131, Italy*
[3]*RIKEN Nishina Center, 2-1 Hirosawa, Wako, Saitama 351-0198, Japan*
[4]*Istituto Nazionale di Fisica Nucleare, Sezione di Napoli, Napoli, Italy*
[5]*Università della Campania Luigi Vanvitelli, I-81100 Caserta, Italy*
[6]*Department of Physics, Kyushu Sangyo University, Fukuoka 813-8503, Japan*
[7]*Grand Accélérateur National d'Ions Lourds, Commissariat à l'Energie Atomique, DRF–, Centre National de la Recherche Scientifique, IN2P3, Bvd Henri Becquerel, F-14076 Caen, France*
[8]*Yukawa Institute for Theoretical Physics, Kyoto University, Kyoto 606-8502, Japan*
[9]*Istituto Nazionale di Fisica Nucleare, Sezione di Milano, I-20133 Milano, Italy*
[10]*CNS, University of Tokyo, Tokyo 351-0198, Japan*
[11]*Department of Physics, University of Tokyo, Hongo7-3-1, Bunkyo-ku, 113-0033 Tokyo, Japan*
[12]*Department of Physics, University of Oslo, N-0316 Oslo, Norway*
[13]*Department of Physics, Rikkyo University, 3-34-1 Nishi-Ikebukuro, Toshima-ku, Tokyo 171-8501, Japan*
[14]*Department of Physics, Osaka University, Osaka 560-0043 Toyonaka, Japan*
[15]*Dipartimento di Fisica dell'Università degli Studi di Milano, I-20133 Milano, Italy*
[16]*School of Computing, Engineering and Mathematics, University of Brighton, Brighton BN2 4JG, England, United Kingdom*
[17]*Institut de Physique Nucléaire, Centre National de la Recherche Scientifique, IN2P3, Université Paris-Sud, Université Paris-Saclay, 91406 Orsay Cedex, France*
[18]*Atomki, H-4001 Debrecen, Hungary*
[19]*Dipartimento di Fisica ed Astronomia dell'Universitá di Firenze and Istituto Nazionale di Fisica Nucleare Firenze, I-50019 Firenze, Italy*
[20]*Instituut voor Kern en Stralings Fysica, K.U. Leuven, B-3001 Heverlee, Belgium*
[21]*Department of Physics, University of Surrey, Guildford GU2 7XH, England, United Kingdom*
[22]*Department of Physics, University of York, Heslington, York YO10 5DD, England, United Kingdom*
[23]*Department of Physics, Tohoku University, Miyagi 980-8578, Japan*
[24]*Instituto de Estructura de la Materia, CSIC, E-28006 Madrid, Spain*
[25]*Departamento de Física Teórica, Universidad Autónoma de Madrid, E-28049 Madrid, Spain*
[26]*IRCNPC, School of Physics and Nuclear Engineering, Beihang University, Beijing 100191, China*
[27]*Department of Physics, Istanbul University, 34134 Istanbul, Turkey*

(Received 29 November 2019; accepted 1 July 2020; published 28 July 2020)

Reduced transition probabilities have been measured for the neutron-rich $^{73,74,75}$Ni nuclei with relativistic Coulomb excitation performed at the RIKEN Nishina Center. For the even-even Ni isotope the determined $B(E2;0^+ \rightarrow 2^+)$ value is compatible within errors with the result of a previous intermediate energy Coulomb excitation experiment, although being somewhat larger. For the odd Ni isotopes $B(E2)$ values have been determined for the first time. In the middle $\nu g_{9/2}$ shell nucleus $^{73}$Ni three peak candidates have been observed and tentatively assigned to the $(5/2^+)$, $(13/2^+)$, and $(11/2^+)$ excitations. Two peak candidates have been observed in $^{75}$Ni and tentatively assigned to the $(13/2^+)$ and $(11/2^+)$ levels. The measured $B(E2)$ values are in line with the large $B(E2)$ reported in $^{70}$Ni and at variance with the small strength measured in $^{72}$Ni. Excitation

*andrea.gottardo@lnl.infn.it

 

energies compare well with the result of large-scale shell-model calculations, while $B(E2)$ values are larger than predicted. This could indicate an increasing contribution of proton excitations across the $Z = 28$ shell closure when approaching $^{78}$Ni.

DOI: 10.1103/PhysRevC.102.014323

## I. INTRODUCTION

One of the most striking features of the atomic nucleus is the fact that, while correlation effects between valence particles can be modeled in an effective way, a comprehensive quantitative description of bulk properties such as binding energies and shell closures is still lacking [1]. This is indeed directly linked to the properties of the nuclear Hamiltonian, which has a central (monopole) part difficult to describe with two-body forces only. As a consequence, many of the recent efforts have been devoted to the understanding of the role played by the different components of the nuclear interaction in determining the shell structure of nuclei.

The Ni isotopes are in this regard a benchmark of nuclear studies, as they correspond to a proton shell closure ($Z = 28$), while also exhibiting neutron shell or subshell closures at $N = 28$ ($^{56}$Ni), $N = 40$ ($^{68}$Ni), and $N = 50$ ($^{78}$Ni). An intriguing interplay among spherical, prolate, and $\gamma$-unstable shapes has been predicted in the Ni isotopes driven by the combined effect of the tensor force and different particle configurations [2–4]. Such configuration-dependent shell structure translates into the coexistence of spherical and strongly deformed shapes with shape fluctuations and with a spectrum approaching the symmetry group $E(5)$ with a behavior which has been interpreted as a striking example of phase transitions in dual quantum liquids [3]. In parallel, with the double magicity of $^{78}$Ni recently assessed [5], there is an interest in studying the filling of the $\nu g_{9/2}$ orbital, the closure of which corresponds to the $N = 50$ gap. Nickel isotopes are an interesting example of partial conservation of the seniority quantum number. Seniority remains a good quantum number for any two-body interaction acting within a single $j$ shell when $j \leqslant 7/2$, but it needs not be conserved for $j \geqslant 9/2$ [6]. Partial conservation of the seniority quantum number—most eigenstates are mixed in seniority but some remain pure—has been recently predicted in nuclei, like the neutron-rich Ni isotopes, filling the $g_{9/2}$ shell [7–9]. Indeed, the seniority classification is a good approximation for $n$-identical nucleons in the $j = 9/2$ shell. Seniority mixing can appear if more than one state with the same $j$ and with different seniority occur at similar excitation energy, but it can be shown that for any reasonable nuclear interaction the off diagonal matrix elements are small compared with the state energy difference [8].

A possible hint of perturbation of the classical seniority-scheme picture came when Perru *et al.* [10] found an unexpectedly high $B(E2; 0^+ \rightarrow 2^+)$ value in $^{70}$Ni from an intermediate energy Coulomb excitation measurement. The authors interpreted the result as evidence of a reduction of the proton $Z = 28$ shell gap when moving towards the $N = 50$ shell closure, a reduction mainly attributed to the tensor component of the nuclear force. In fact, such component of the nuclear force determines a repulsive interaction between the $\nu g_{9/2}$ and the $\pi f_{7/2}$ shells, and in contrast an attractive force between the $\nu g_{9/2}$ and the $\pi f_{5/2}$ shells [2]. This in turn determines a decrease of the $Z = 28$ gap as more neutrons are added in the $\nu g_{9/2}$ orbits towards $^{78}$Ni. The immediate consequence of this level shift is a decrease in the energy cost of proton excitations from the $Z = 28$ core to the shells above with an increase in collectivity of the first-excited $2^+$ level. As a result, the augmented collectivity observed in Ref. [10] was taken as a signature of a reduced shell gap at $Z = 28$ approaching $N = 50$. Moreover, recent radioactivity studies in $^{70}$Co and $^{70}$Ni showed that shape coexistence occurs in the isobaric $A = 70$ chain due to type-II shell evolution [11]. In a recent remeasurement of the $B(E2; 0^+ \rightarrow 2^+)$ of $^{70}$Ni [12], the authors found a result smaller than but still compatible within errors with Ref. [10]. In more neutron-rich nuclei, two inelastic proton scattering experiments performed for $^{74}$Ni also yielded a large deformation parameter [13,14], interpreted as a sign of enhanced quadrupole collectivity. The suggestion of a reducing $Z = 28$ gap in neutron-rich Ni nuclei seems to be in contrast with the results of two measurements probing the collectivity of the first-excited $2^+$ level in the $^{72,74}$Ni isotopes based either on the measured lifetime of such state ($^{72}$Ni) [15] or on an intermediate energy Coulomb excitation ($^{74}$Ni) [16].

To clarify this issue we have investigated the $B(E2)$ values of the even-even $^{74}$Ni nucleus and of the odd $^{73,75}$Ni isotopes ($^{75}$Ni is presently the most neutron-rich Ni isotope experimentally reachable with this approach), under the assumption that the observed collectivity is representative of that of the even-even core nuclei.

## II. EXPERIMENTAL SETUP

The experiment was performed at the Radioactive Isotope Beam Factory (RIBF), operated jointly by the RIKEN Nishina Center and the Center for Nuclear Study of the University of Tokyo. It was run together with $\beta$-decay spectroscopy measurements to optimize the beam time usage. The radioactive ions $^{73,74,75}$Ni were produced by the fission of a primary $^{238}$U beam. The beam was delivered by the RIBF accelerator complex at an energy of 345 MeV/nucleon, with an average intensity of 10 pnA. The $^{238}$U ions impinged on a 3-mm-thick Be target at the F0 focus of the BigRIPS fragment separator and the resulting fission fragments were selected using the $B\rho - \Delta E - B\rho$ method [17]. The selection and measurement of the mass-to-charge ratio $A/Q$ were performed using the time-of-flight (TOF) information, based on the response of two plastic scintillators placed at the focal points F3 and F7, and the determination of the magnetic rigidity obtained from the measurement [with parallel plate avalanche counters (PPACs)] of the position and angle at the achromatic

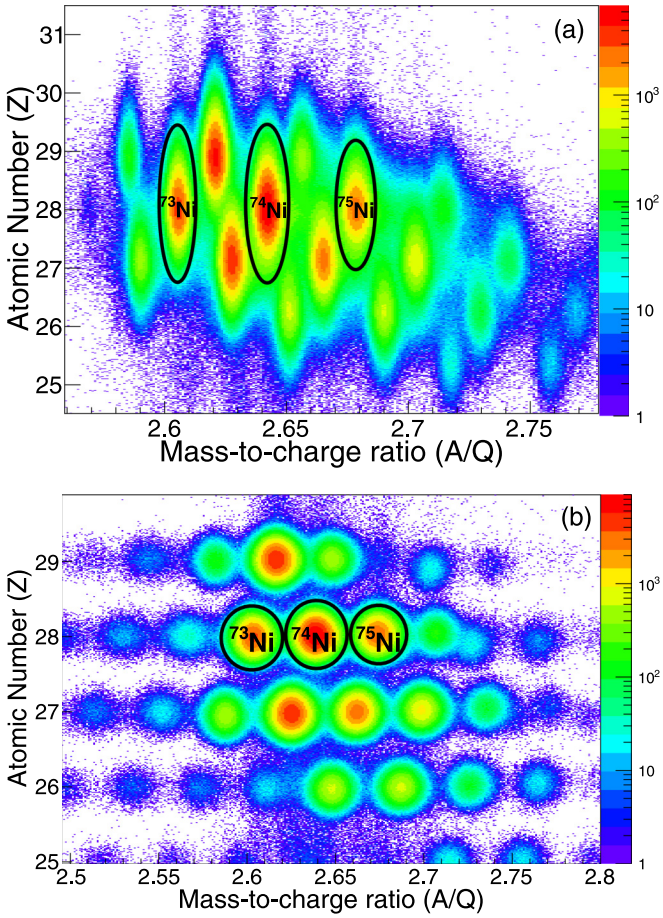


FIG. 1. (a) Identification plot obtained from the BigRIPS fragment separator, providing an image of the cocktail beam arriving on the secondary target for Coulex. (b) Identification plot obtained from the ZeroDegree fragment separator, after secondary target. In both graphics the atomic number $Z$ is in the ordinate, while the abscissa represents the mass-to-charge ratio $A/Q$. The $^{73,74,75}$Ni isotopes are pointed out.

focal point F3 and at the dispersive focal point F5 [18]. The momentum acceptance of the separator was 4.8%. The atomic number $Z$ of the fragments was measured thanks to a ionization chamber located at the focal point F7, via energy loss in the gas. The ions resulting from primary beam fission were thus identified on an event-by-event basis in both $A/Q$ and $Z$. Figure 1(a) shows the identification plot obtained from the BigRIPS fragment separator. The Ni isotopes are pointed out, the most intense being $^{74}$Ni.

This secondary beam was then delivered to a 1.177-g/cm$^2$ natural Pb target located at the F8 focal point. The energy of the $^{74}$Ni ions at the central target position was on average 215 MeV/nucleon, while their trajectories before and after the lead target were reconstructed using three double PPACs detectors, two located upstream and one downstream with respect to the target. The PPACs position resolution in $X$ and $Y$ was 0.5 mm, allowing for a scattering angle resolution of about 5 mrad, to be compared with the about 6-mrad angular straggling of the $^{74}$Ni ions inside the secondary target, calculated using the ATIMA code [19].

Reaction products were identified in the downstream ZeroDegree spectrometer [17], which also transported them to the WAS3Abi-EURICA (see Refs. [20,21], respectively) setup for decay spectroscopy studies. This spectrometer, like BigRIPS, can identify the reaction products in $A/Q$ and $Z$ using TOF, beam trajectory, and energy loss information. Figure 1(b) shows the identification plot obtained from the ZeroDegree fragment separator. The loci corresponding to the $^{73,74,75}$Ni ions are marked. Incidentally, the simultaneous performance of Coulomb excitation and decay-spectroscopy measurements implied to maximize the transmission of the ions of interest to the WAS3Abi-EURICA setup (decay spectroscopy), mainly Mn, Fe, and Co isotopes. This essentially translated in the necessity to keep the beam energy at the secondary target point quite high, if compared to previous Coulomb excitation experiments [22], corresponding to a lower Coulomb excitation cross section.

In order to detect the $\gamma$ rays emitted by the decay of the Coulomb-excited levels in the isotopes of interest, the DALI2 [23] NaI(Tl) scintillator array was placed around the Pb secondary target. The array was composed of 186 scintillators covering center-of-crystal angles from 19° to 150°. A GEANT4 [24] simulation of the DALI2 spectrometer was performed and validated with efficiency measurements using $^{60}$Co and $^{137}$Cs sources. A 5%-level agreement was found between the measured and simulated spectra.

## III. EXPERIMENTAL RESULTS

The Coulomb-excited Ni residues had a velocity of about 0.6$c$, and thus the Lorentz boost implied a strong forward focusing of the emitted $\gamma$ rays. As a consequence, only the most forward NaI(Tl) crystals were used for the analysis, at angles $<69°$. This was also instrumental in allowing a cut on the beam-induced background since at forward angles $\gamma$ rays from reaction products are Doppler shifted at higher energies, where the background is smaller. The $\gamma$ rays decaying from the states of interest were then selected applying a gate on the Ni isotopes in both BigRIPS and ZeroDegree. Part of the background at low energy will also originate from the Compton scattering of high-energy $\gamma$ rays coming from the excited $^{208}$Pb $3^-$ and $2^+$ states. A Doppler correction was applied to the $\gamma$-ray spectrum, taking into account the average beam energy (215 MeV/nucleon) and the angles between the detected photon and the emitting fragment, assuming the reaction residues having a direction on the beam axis. Figure 2 shows the experimental $\gamma$-ray spectra from the decay of the Coulomb-excited states in the $^{73,74,75}$Ni isotopes.

In the $^{74}$Ni spectrum the $2^+$ state at 1009(15) keV, known from previous $\beta$-decay experiments [1024(1) keV] and from Refs. [13,16], is clearly visible. For the $^{73,75}$Ni isotopes, the spectra show more complex structures with peaks located at an excitation energy of $\approx$1 MeV. Further guidance in the identification of peaks is provided by $\gamma$ spectra when a multiplicity of 1 is required: they are shown in the insets of Fig. 2. In fact, relativistic-energy Coulomb excitation is primarily a $\gamma$ multiplicity-1 process, while background from beam-matter interaction engenders higher multiplicity. Therefore, the $\gamma$ spectra so conditioned should have an improved

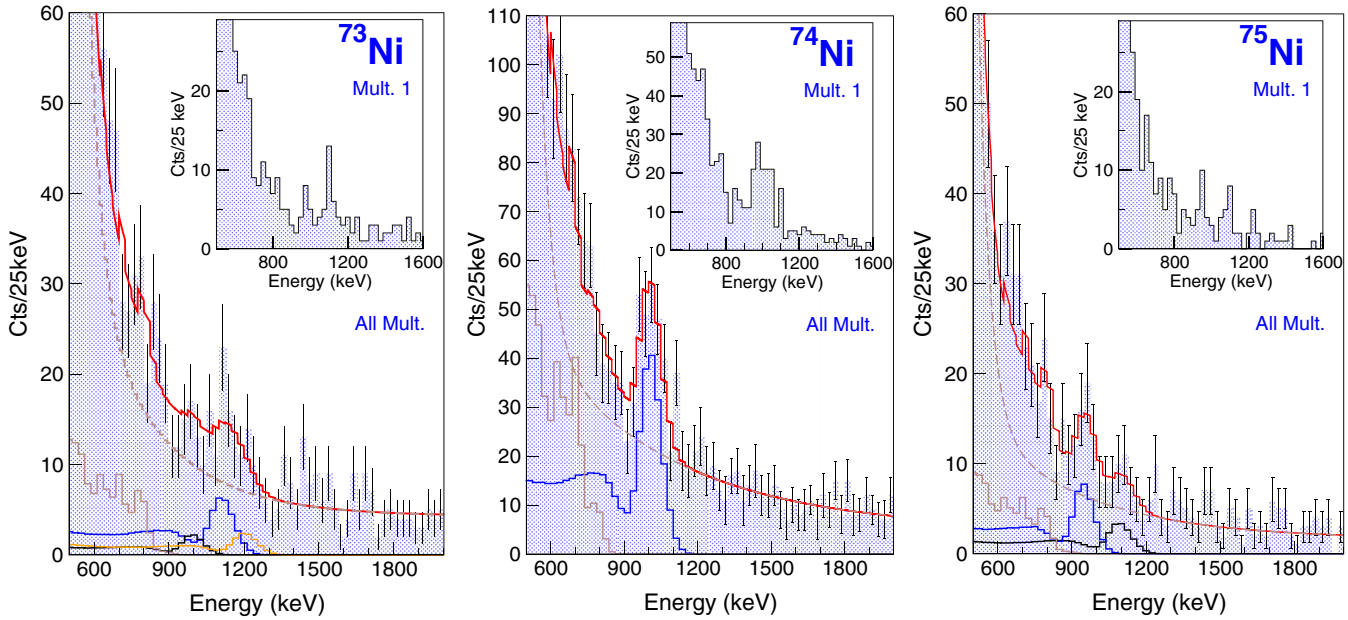


FIG. 2. Gamma-ray spectra from relativistic Coulomb excitation of $^{73,74,75}$Ni after selection on the corresponding ions on both incoming and outgoing secondary beams. The error bars are indicated in the plot. The brown dashed lines represent the simulations for the background, constituted of two exponentials. The Coulomb excitation of the $2^+$ of the target isotope $^{206}$Pb is drawn with a continuous brown line. The black and blue lines are the response functions for the Coulomb excitation of the selected Ni isotopes. All these simulation functions are then fitted to the experimental spectrum, as shown by the red continuous line. In the insets the spectra with a $\gamma$ multiplicity-1 condition are presented.

peak to background at the expense of some statistics loss. This is indeed the case for the spectra for Ni isotopes: in $^{73}$Ni three transitions are visible at 992(20), 1115(20), and 1210(25) keV whereas two transitions are observed in $^{75}$Ni, at 950(20) and 1101(20) keV. They correspond in energy to the structures barely identifiable in the multiplicity-ungated spectra.

In order to extract the Coulomb excitation cross sections, one has to determine the intensities of the $\gamma$ transitions observed. This requires the knowledge of the absolute $\gamma$ efficiency of the DALI2 detector and to take into account the Lorentz boost (forward focusing) of the emitted radiation. Furthermore, the Doppler broadening and the Compton edges of transitions lying higher in energy alter the normal Gaussian shape of the peaks. All these effects can be consistently treated only with a simulation. The $\gamma$ spectra were simulated using the GEANT4 code, employing as inputs the energies of the $2^+$ state of $^{74}$Ni and of the identified states in $^{73}$Ni and in $^{75}$Ni, the measured energy resolution for each scintillator, the average beam velocity, and the lead target thickness. A similar simulation was performed for the excitation of the $^{206}$Pb nuclei in the target, whereas the excited states of $^{208}$Pb are too high in energy to give a contribution. The simulated $^{206}$Pb Coulomb excitation process gives origin to a very large bump at 500–800 keV, since the Doppler correction is based on the Ni kinematics (see the continuous brown lines in Fig. 2). In order to compare these calculations with the experimental data, a double exponential background plus a constant was added to the simulated spectra, as a model of the atomic and beam-related background. The resulting function was fitted to the $\gamma$-ray spectra as shown in Fig. 2, with a $\chi^2$ minimization. The cross section of the excitation process was extracted from the fitting constant used for the simulated Ni spectra. A cross section of $\sigma = 118$ mbarn is determined for $^{74}$Ni. The statical error coming from the $\chi^2$ minimization is 16 mbarn, or about 14%. The error considered for the thickness of the secondary target is about 1%. As mentioned before, the Monte Carlo simulation of the $\gamma$ efficiency agreed within 5% with the experimentally derived efficiency, estimated with a $^{60}$Co source of known activity. Therefore, an additional systematic 5% error was included in the cross-section estimate. Overall, the cross section measured for the $2^+$ state in $^{74}$Ni is $\sigma(0^+ \rightarrow 2^+) = 118 \pm 20$ mbarn.

For the odd-$A$ nuclei, the extraction of the $\gamma$ intensities and hence of the Coulex cross sections is less straightforward due to both theoretical and experimental issues. Experimentally, the difficulty for $^{73,75}$Ni is due to the low statistics, which makes the $\chi^2$ minimization quite unstable. As for the case of peak identification, the multiplicity-1 spectra provide essential guidance in determining the rough values of the intensities, which are necessary to set the limits of the parameters needed by the fit with the simulated response functions. Employing this procedure, the $^{73,75}$Ni experimental cross sections were determined relatively to the one of $^{74}$Ni. Figure 2 shows the fit with the response function for observed transitions for odd isotopes. The cross sections for the excitation of the $^{73}$Ni states are $\sigma$ (state at 992 keV)$= 18^{+20}_{-18}$ mbarn, $\sigma$ (state at 1115 keV) $= 38 \pm 15$ mbarn, and $\sigma$ (state at 1210 keV) $= 18 \pm 10$ mbarn, and those for $^{75}$Ni are $\sigma$ (state at 1101 keV) $= 29 \pm 20$ mbarn and $\sigma$ (state at 950 keV) $= 36 \pm 23$ mbarn.

The statistical significance of the measured peaks has been determined following the ISO/TC 69 standard. It ranges from

about 21 in the case of $^{74}$Ni to about 3.8 and 1.8 for the 1115-, 1210-, and 992-keV $\gamma$-ray lines in $^{73}$Ni, respectively. For the $^{75}$Ni case the significance is 4.5 and 2.5 for the 950- and 1101-keV $\gamma$ rays, respectively. For the case where the statistical significance is below 3, the identification of $\gamma$ rays presented in this paper should be considered tentative and the state energies will be indicated between parentheses in the following.

The cross section of the excitation process was extracted from the fitting constant used for the simulated Ni spectra. It must be noted that these cross sections include both electromagnetic and nuclear contributions. Therefore, a calculation with both nuclear and electromagnetic excitations is demanded in order to extract the $B(E2)$ value for the observed excited states. With the aim of determining the nuclear contribution, we started first with $^{74}$Ni, where a previous $B(E2)$ measurement is available in Ref. [16].

The calculation to derive the $B(E2)$ value follows the procedure described in Ref. [25]. In that paper the authors made a detailed analysis of the effects that scattering angle resolution and straggling can have on the comparison between the measured and the theoretical cross section. In particular, the theoretical differential cross section obtained from nuclear and Coulomb potential scattering must be convoluted with the experimental scattering angle resolution and straggling in target in order to be compared with the result of the measurement. It was also pointed out that the code FRESCO [26,27] can properly treat not only Coulomb and nuclear scattering, but also their interference. As a consequence, the total (nuclear and Coulomb) cross section for the present experiment is calculated using this code. The nuclear potential model employed is derived from Ref. [28], calculated for the $^{74}$Ni and $^{208}$Pb collision. The CEG07 interaction [29] and Sao Paulo density [30] were used. A recent $^{74}$Ni$(p, p')$ $^{74}$Ni measurement performed at RIKEN [14] determined a deformation length $\delta = 0.9(2)$ fm for $^{74}$Ni. This value is used as an input to the FRESCO calculation. For the Coulomb part, the quadrupole matrix element is a free parameter that is varied to reproduce the experimental cross section. It is found that the interference between the nuclear and the Coulomb potentials is destructive and that it almost cancels the nuclear contribution. Considering the large experimental errors (see later), the final result on the $B(E2)$ value is independent of the deformation length chosen on a wide range. Using these parameters with the code FRESCO, we obtained a differential total (nuclear plus Coulomb) cross section which was then convoluted with the straggling in target and scattering angle resolution from focal plane detector position accuracy. This amounts to about a 7-mrad scattering angle Gaussian smearing. The result of this procedure can be compared with the experimental data after the beam transmission from BigRIPS to ZeroDegree is folded with the smeared differential cross section. Overall, losses due to transmission acceptance were below 10%.

Following the aforementioned strategy, the measured cross section of $\sigma_n + \sigma_c = 118(19)$ mb in $^{74}$Ni could be reproduced from FRESCO calculations employing an $E2$ transition matrix element $M_p = 33.2\ e\,\mathrm{fm}^2$ which corresponds to a $B(E2; 0^+ \rightarrow 2^+) = 1133\ e^2\mathrm{fm}^4$. This value has to be corrected for the feeding from higher-lying states [22] which may be populated by single-step Coulomb and nuclear excitations. The $\gamma$ decay of these predominantly $2^+_x$ and $3^-_x$ levels will in fact increase the observed intensity of the $2^+ \rightarrow 0^+$ transition. Previous Coulomb excitation studies on Sn nuclei in similar experimental conditions estimated a contribution to the $B(E2; 0^+ \rightarrow 2^+)$ value ranging from $14 \pm 7$ to $21 \pm 11\%$ [22,25,31]. In the present paper, we consequently employ a $20 \pm 10\%$ estimate for the feeding, yielding $B(E2; 0^+ \rightarrow 2^+) = 906\ e^2\mathrm{fm}^4$ for $^{74}$Ni.

The same procedure is then applied to evaluate the $B(E2)$ from the total cross sections of the odd-even $^{73,75}$Ni isotopes. It is assumed that their scattering length is the same as for $^{74}$Ni. The near cancellation of nuclear potential and nuclear-Coulomb potential interference contributions assures that this assumption does not impact the final result within the large statistical errors from measurement.

Errors on $B(E2)$ values were estimated propagating the error from the measured cross sections, considering that Coulomb cross section is a linear function of $B(E2)$. The 20% feeding estimate is considered to have a 50% relative error, which is quadratically summed to the error coming from the cross-section measurement. A further systematic error of 10% is introduced as a result of the uncertainty linked to the choice of the nuclear potential to be used in the FRESCO calculation. This error estimate was obtained by comparing the result from the aforementioned potential with those from a Woods-Saxon and a $t - \rho\rho$ potential as implemented in the code DWEIKO [32]. For $^{74}$Ni, this leads to $B(E2; 0^+ \rightarrow 2^+) = 906 \pm 222\ e^2\mathrm{fm}^4$. The result from a recent intermediate energy Coulomb excitation measurement for $^{74}$Ni, reported in Ref. [16], is $B(E2; 0^+ \rightarrow 2^+) = 642 \pm 220\ e^2\mathrm{fm}^4$, obtained without subtracting a feeding from higher-lying levels.

The results for the odd-even isotopes are reported in Tables I and II.

## IV. DISCUSSION OF RESULTS

Nuclear structure arguments can help to make tentative assignments for the spin parity of these states. The ground state of $^{73,75}$Ni is supposed to be $I^\pi = (9/2^+)$, considering the unpaired neutron located in the $\nu g_{9/2}$ shell. Schematically, the relativistic Coulomb excitation will then break a pair of neutrons in the same $\nu g_{9/2}$ orbit, coupling them to the unpaired neutron giving rise to a multiplet of states. Later in the text, it will be shown that shell-model calculations predict that among all the states coming from the multiplet $(g_{9/2})^n$ the $5/2^+$, $13/2^+$, and $11/2^+$ levels are expected to be at excitation energies around 1 MeV for both nuclei, the $13/2^+$ having the larger $B(E2)$ among the three. The other states where considerable $E2$ strength is predicted, like $7/2^+$, are expected to be located at much lower excitation energy and therefore in the region of the experimental spectrum strongly polluted by target excitations. For $^{73}$Ni two $5/2^+$ levels are predicted by the calculations at energies around 500 and 850 keV whereas only this second one is expected for $^{75}$Ni. From previous works a $(7/2^+)$ state is known in $^{73}$Ni at 239 keV of excitation energy and a $(5/2^+)$ level at 524 keV [33]. Nothing is known for $^{75}$Ni. We therefore tentatively

TABLE I. Measured values for the energy of excited states in $^{73,74,75}$Ni in comparison with theoretical predictions. SM1 is a shell model based on a unified realistic interaction employing the pairing plus multipole Hamiltonian and a universal monopole, while SM2 is a shell-model calculation using the CD-Bonn potential. A calculation using a single $g_{9/2}$ shell (seniority scheme) is also presented for reference. See text for details.

| | $E_x$ $2^+$(keV) | | | | | | | | | | | |
|---|---|---|---|---|---|---|---|---|---|---|---|---|
| | Measured | | | | SM1 | | | | SM2 | | | |
| $^{74}$Ni | 1009(15) | | | | 1074 | | | | 991 | | | |
| | Single orbit | | | | | | | | 1070 | | | |
| | $E_x$ $(5/2^+)$ (keV) | | | | $E_x$ $(13/2^+)$ (keV) | | | | $E_x$ $(11/2^+)$ (keV) | | | |
| | Measured | SM1 | SM2 | Single orbit | Measured | SM1 | SM2 | Single orbit | Measured | SM1 | SM2 | Single orbit |
| $^{73}$Ni | [992(20)] | 1223 | 842 | 938 | 1115(20) | 1123 | 1008 | 1213 | 1210(25) | 1298 | 1237 | 1398 |
| $^{75}$Ni | | | | | 950(20) | 1199 | 1061 | 1152 | [1101(20)] | 1217 | 1173 | 1271 |

assume the three transitions in $^{73}$Ni at 992(20), 1115(20), and 1210(25) keV to deexcite the $(5/2^+)$, $(13/2^+)$, and $(11/2^+)$ states at 992(20), 1115(20), and 1210(25) keV of excitation energy, respectively. In the case of the $^{75}$Ni isotope, the two transitions observed at 950(20) and 1101(20) keV are also tentatively assumed to deexcite corresponding states of spin parity $(13/2^+)$ and $(11/2^+)$, respectively. We point out here that the $j-1$ anomaly observed in the $^{77}$Zn isotone, which has a $7/2^+$ ground state, is not predicted by shell models for $^{75}$Ni. Hence, we keep the assumption that the $^{75}$Ni ground state has a $9/2^+$ spin and parity.

The huge shoulder at lower energies in Fig. 2, reaching up to about 700 keV, is coming from the aforementioned atomic background and also includes the $2^+$ excitation of $^{206}$Pb at 800 keV, present with a 24% percentage in the natural Pb target. Table I presents a summary of the measured excited states together with the results of theoretical calculations.

From the theoretical point of view, core-excitation coupled states are expected to carry the $E2$ strength in $^{73,75}$Ni. For $^{73}$Ni, the coupling of an odd $g_{9/2}$ neutron to the $^{72}$Ni $2_1^+$ state would give rise to a quintet of states with spin values $5/2^+$, $7/2^+$, $9/2^+$, $11/2^+$, and $13/2^+$, with a total $\sum_J B(E2; 9/2^+ \rightarrow J) \approx B(E2\uparrow)_{^{72}\mathrm{Ni}}$. Here the sign $\approx$ is related to the expected anharmonicities coming from the "blocking" of the odd neutron. Shell-model calculations performed using the $V_{\text{low-k}}$ approach [34] or a unified realistic Hamiltonian with a monopole based universal force [35] show that almost 90% of the strength is exhausted by the $5/2^+$, $13/2^+$, and $11/2^+$ members of the multiplet, with the $13/2^+$ state giving the dominant contribution (see below for shell-model calculations).

It is interesting to compare the experimental results with the predictions of large-scale shell-model calculations using effective interactions which are now available for this mass region. Shell-model calculations have been performed using SM1, a unified realistic interaction employing the pairing plus multipole Hamiltonian combined with the monopole interaction constructed starting from the monopole-based universal force from Refs. [35,36], or SM2, an effective Hamiltonian derived from the CD-Bonn potential, renormalized by way of the $V_{\text{low-k}}$ approach [37], within the framework of the time-dependent perturbation theory [34].

In the model (1), SM1, the model space is composed of the $f_{7/2}$, $p_{3/2}$, $f_{5/2}$, $p_{1/2}$, $g_{9/2}$, and $d_{5/2}$ orbitals for both protons and neutrons. The large-scale shell-model calculations are performed under the truncation that protons and neutrons are not excited from the $f_{7/2}$ and the $p_{3/2}$ orbitals. The interaction matrix elements and the single-particle energies are given in the same way as the derivation of the Hamiltonian in the previous papers [35,38], where the effective charges for proton and neutron are taken as $e_p = 1.50e$ and $e_n = 0.75e$. In model (2), SM2, a different valence space was considered,

TABLE II. Measured values for the $B(E2)\downarrow$ strengths in $^{73,74,75}$Ni in comparison with theoretical predictions. SM1 is a shell model with a unified realistic interaction employing the pairing plus multipole Hamiltonian and a universal monopole, while SM2 is a calculation using the CD-Bonn potential. A $g_{9/2}$ seniority-scheme calculation is also presented for reference. See text for details.

| | $B(E2; 2^+ \rightarrow 0^+)$ $(e^2\mathrm{fm}^4)$ | | | | | | | | | | | |
|---|---|---|---|---|---|---|---|---|---|---|---|---|
| | Measured | | | | SM1 | | | | SM2 | | | |
| $^{74}$Ni | $181 \pm 44$ | | | | 120 | | | | 106 | | | |
| | Single orbit | | | | | | | | 113 | | | |
| | $B(E2; (5/2^+) \rightarrow 9/2^+)$ $(e^2\mathrm{fm}^4)$ | | | | $B(E2; (13/2^+) \rightarrow 9/2^+)$ $(e^2\mathrm{fm}^4)$ | | | | $B(E2; (11/2^+) \rightarrow 9/2^+)$ $(e^2\mathrm{fm}^4)$ | | | |
| | Measured | SM1 | SM2 | Single orbit | Measured | SM1 | SM2 | Single orbit | Measured | SM1 | SM2 | Single orbit |
| $^{73}$Ni | $237^{-267}_{-237}$ | 87 | 85 | 107 | $217 \pm 94$ | 106 | 116 | 116 | $117 \pm 69$ | 47 | 33 | 63 |
| $^{75}$Ni | | | | | $202 \pm 134$ | 71 | 78 | 85 | $191 \pm 136$ | 32 | 40 | 50 |

with protons in the $f_{7/2}$, $p_{3/2}$, and $f_{5/2}$ shells and neutrons in the $p_{3/2}$, $f_{5/2}$, $p_{1/2}$, and $g_{9/2}$ orbitals. The electromagnetic transition strengths were calculated by using proton and neutron effective $E2$ operators consistently derived with the same perturbation approach of the Hamiltonian. A calculation based only on the $\nu g_{9/2}$ shell was also performed to provide a reference. In this model the $B(E2)$ values were normalized to the average of the $2^+ \rightarrow 0^+$ $E2$ strengths in $^{74}$Ni predicted by SM1 and SM2. The excited levels predicted by the three calculations are compared to experimental values in Table I. The corresponding theoretical $B(E2)$ strengths for $^{74,73,75}$Ni are shown in Table II.

For the even-even nucleus $^{74}$Ni, SM1, SM2, and single-orbit calculations agree very well with the experimental results regarding the excitation energy of the $2^+$ level. In contrast, the $B(E2)$ strength appears to be underestimated by models.

Concerning the odd isotopes, the limited statistics prevents a firm comparison as in the case of $^{74}$Ni, but some considerations can be drawn from data. For $^{73}$Ni both shell-model and single-orbit calculations predict as low-lying excitations above the $9/2^+$ ground state the $7/2^+$ and $5/2^+_1$ states and at about 1 MeV of excitation energy (the region of interest for this measurement) the $5/2^+_2$, $13/2^+$, and $11/2^+$ levels. Overall, the calculated excitation energies for those states are in agreement with the experimental observations. For the tentatively assigned $(13/2^+)$ and $(11/2^+)$ states, the measured transition strengths are also larger than the results of SM1, SM2, and single-orbit calculations, although the large error bars prevent one from drawing a definitive conclusion. The similarity with the $^{74}$Ni case is anyway suggestive of a common trend. Both shell-model and single-orbit calculations predict in $^{73}$Ni two $5/2^+$ levels at around 300 and 900 keV of excitation energy. The first one may indeed be the one reported in Ref. [33]. The $B(E2; 5/2^+_1 \rightarrow 9/2^+)$ is calculated between zero (single orbit) and few $e^2\text{fm}^4$ (shell-model) whereas the $B(E2; 5/2^+_2 \rightarrow 9/2^+)$ is predicted of the order of about 100 $e^2\text{fm}^4$. This large difference in transition strength to the ground state is a consequence of seniority conservation. The $5/2^+_1$ level has a dominant component with seniority $\nu = 5$ (two broken neutron pairs in the corresponding even-even nucleus) and therefore, due to the seniority change of $\Delta\nu = 4$, the transition to the seniority $\nu = 1$ ground state is hindered. The $5/2^+_2$ level, in contrast, is dominantly a seniority $\nu = 3$ state (one broken neutron pair in the corresponding even-even nucleus) allowing an $E2$ decay to the ground state. Even if seniority need not be conserved for shells with $j \geqslant 9/2$, it has been shown recently that for $n = 4$ identical nucleons in a $j = 9/2$ shell there are two $J = 4$ states with seniority $\nu = 2$ and 4, which do not mix for any interaction [8]. The same holds for $J = 6$ states. A similar situation occurs in the odd-$A$ isotope $^{73}$Ni, which has the $g_{9/2}$ shell half filled with neutrons. Because of particle-hole symmetry no mixing can occur between states differing by two units of seniority [39] and, specifically, the $5/2^+_1$ and $5/2^+_2$ states cannot mix. Limited mixing is therefore expected for the two $5/2^+$ states of $^{73}$Ni. This mechanism of nonmixing holds only in a single-shell scenario and is expected to break down if the levels with the same $J$ are close in energy. For example, the two $11/2^+$ levels, predicted close in energy (within less than 100 keV), display a seniority mixing of almost 50%. Both SM1 and SM2 and the single-orbit calculation predict a $B(E2; (5/2^+) \rightarrow 9/2^+)$ value which is smaller than the observed one, even though the large experimental error again precludes a quantitative comparison. For $^{75}$Ni, both shell-model calculations and the single-orbit model predict the $13/2^+$ level to be at lower excitation energy than the $11/2^+$ level. The energies match those of the experimentally observed $\gamma$ rays. The two observed $B(E2)$ values are somehow larger than the shell-model results, confirming the trend already present in $^{73,74}$Ni.

The nonobservation in $^{75}$Ni of the $(5/2^+) \rightarrow 9/2^+$ transition, apart from intensity considerations related to the low production rate of this isotope, is possibly linked to the opening of alternative decay paths for this level (an example is the decay of the $5/2^+_2$ to $7/2^+$), which are likely to be hindered in $^{73}$Ni. For the latter nucleus, located just in the middle of the $g_{9/2}$ shell, under the assumption of seniority conservation, transitions between states with the same seniority should indeed be forbidden.

Overall, for all three nuclei the observed level scheme and $B(E2)$ trend, when compared to the shell-model results and to the predictions of a single-orbit calculation based on $g_{9/2}$, show that the latter orbital is dominating the valence structure of the neutron-rich nuclei $^{73,74,75}$Ni. However, since the measured collectivity is larger than the theoretical expectations, one may speculate that the contribution of proton excitations across $Z = 28$, enhancing the $E2$ strength, could be underestimated by the present models. Indeed, the steep rise with respect to the $B(E2)$ values in Ref. [15] may indicate that more important proton contributions are coming into play when approaching the $N = 50$ shell gap.

## V. CONCLUSIONS

In conclusion, we have studied the quadrupole collectivity in the neutron-rich $^{73,74,75}$Ni isotopes via relativistic Coulomb excitation measurements. $B(E2)$ values have been determined for low-lying states in the odd-Ni isotopes for the first time, suggesting a large $B(E2)$ trend, with respect to $^{70}$Ni, at variance with what was measured in $^{72}$Ni. Comparison with shell-model calculations using either the $fpgd$ model space both for protons and neutrons and a unified realistic interaction constructed from the monopole-based universal force or the $pf$ model space both for protons and neutrons and employing an effective Hamiltonian derived from the CD-Bonn potential renormalized by the $V_{\text{low-k}}$ approach and with calculations based on a single neutron orbital shows in general a good agreement for the excitation energies of the states, whereas transition strengths are underestimated. The global decay pattern observed nicely reflects the general expectation based on partial conservation of seniority predicted for nuclei within

the $j = 9/2$ shell. The present results are at variance with the small $B(E2)$ value found in $^{72}$Ni [15] and are somewhat larger than the previous $^{74}$Ni measurement [16]. The fact that the transition strengths are systematically larger than the neutron-space shell-model predictions could suggest that proton excitations across $Z = 28$ may play a more important role than predicted in the wave function of low-lying states when approaching $^{78}$Ni. In particular, the increase of the $B(E2)$ values with respect to $^{72}$Ni could indicate that, starting from the mid-$\nu g_{9/2}$ shell, the $Z = 28$ gap is gradually becoming more susceptible to particle-hole excitations. Another possibility to consider is an increase of excitations across the $N = 50$ shell closure. It remains for future experiments to verify this trend with more precise measurements, also extending them to the more exotic $^{76,77}$Ni isotopes.

## ACKNOWLEDGMENTS

The excellent work of the Riken-Nishina Center accelerator staff is acknowledged. We acknowledge the support of Istituto Nazionale di Fisica Nucleare, Italy. We also acknowledge the National Research, Development, and Innovation Fund of Hungary (Project No. K128947); the European Regional Development Fund (Contract No. GINOP-2.3.3-15-2016-00034); and the National Research, Development, and Innovation Office (NKFIH Contract No. PD124717).

[1] E. Caurier, G. Martinez-Pinedo, F. Nowack, A. Poves, and A. P. Zuker, Rev. Mod Phys. **77**, 427 (2005).
[2] T. Otsuka, T. Suzuki, M. Honma, Y. Utsuno, N. Tsunoda, K. Tsukiyama, and M. Hjorth-Jensen, Phys. Rev. Lett. **104**, 012501 (2010).
[3] T. Otsuka and Y. Tsukoda, J. Phys. (London) **G43**, 024009 (2016).
[4] Y. Tsunoda, T. Otsuka, N. Shimizu, M. Honma, and Y. Utsuno, Phys. Rev. C **89**, 031301(R) (2014).
[5] R. Taniuchi *et al.*, Nature (London) **569**, 53 (2019).
[6] I. Talmi, *Simple Models of Complex Nuclei: The Shell Model and Interacting Boson Model* (Harward Academic, Chur, 1993).
[7] A. Escuderos and L. Zamick, Phys. Rev. C **73**, 044302 (2006).
[8] P. Van Isacker and S. Heinze, Phys. Rev. Lett. **100**, 052501 (2008).
[9] A. I. Morales *et al.*, Phys. Lett. B **781**, 706 (2018).
[10] O. Perru *et al.*, Phys. Rev. Lett. **96**, 232501 (2006).
[11] A. I. Morales *et al.*, Phys. Lett. B **765**, 328 (2017).
[12] O. Wieland *et al.*, Phys. Rev. C **98**, 064313 (2018).
[13] N. Aoi *et al.*, Phys. Lett. B **692**, 302 (2010).
[14] M. L. Cortes *et al.*, Phys. Rev. C **97**, 044315 (2018).
[15] K. Kolos *et al.*, Phys. Rev. Lett. **116**, 122502 (2016).
[16] T. Marchi *et al.*, Phys. Rev. Lett. **113**, 182501 (2014).
[17] T. Kubo *et al.*, Prog. Theor. Exp. Phys. **2012**, 03C003 (2012).
[18] H. Kumagai, A. Ozawa, N. Fukuda, K. Sümmerer, and I. Tanihata, Nucl. Instrum. Meth. A **470**, 562 (2001).
[19] H. Wollersheim *et al.*, Nucl. Instr. Meth. A **537**, 637 (2006).
[20] S. Nishimura, Prog. Theor. Exp. Phys. **2012**, 03C006 (2012).
[21] P.-A. Söderström *et al.*, Nucl. Instr. Meth. B **317**, 649 (2013).
[22] P. Doornenbal *et al.*, Phys. Rev. C **90**, 061302(R) (2014).
[23] S. Takeuchi *et al.*, RIKEN Accelerator Progress Report **36**, 148 (2003).
[24] S. Agostinelli *et al.*, Nucl. Instr. Meth. A **506**, 250 (2003).
[25] V. Vaquero *et al.*, Phys. Rev. C **99**, 034306 (2019).
[26] I. Thompson, Comput. Phys. Rep. **7**, 3 (1988).
[27] http://fresco.org.uk
[28] T. Furumoto, Y. Sakuragi, and Y. Yamamoto, Phys. Rev. C **82**, 044612 (2010).
[29] T. Furumoto, Y. Sakuragi, and Y. Yamamoto, Phys. Rev. C **78**, 044610 (2008).
[30] L. C. Chamon, B. V. Carlson, L. R. Gasques, D. Pereira, C. De Conti, M. A. G. Alvarez, M. S. Hussein, M. A. C. Ribeiro, E. S. Rossi, Jr., and C. P. Silva, Phys. Rev. C **66**, 014610 (2002).
[31] B. Elman *et al.*, Phys. Rev. C **96**, 044332 (2017).
[32] C. A. Bertulani, C. M. Campbell, and T. Glasmacher, Comp. Phys. Comm. **152**, 317 (2003).
[33] M. M. Rajabali *et al.*, Phys. Rev. C **85**, 034326 (2012).
[34] L. Coraggio, A. Covello, A. Gargano, and N. Itaco, Phys. Rev. C **89**, 024319 (2014).
[35] K. Kaneko, T. Mizusaki, Y. Sun, and S. Tazaki, Phys. Rev. C **89**, 011302(R) (2014).
[36] M. Dufour and A. P. Zuker, Phys. Rev. C **54**, 1641 (1996).
[37] S. Bogner, T. T. S. Kuo, L. Coraggio, A. Covello, and N. Itaco, Phys. Rev. C **65**, 051301(R) (2002).
[38] K. Kaneko, T. Mizusaki, Y. Sun, and S. Tazaki, Phys. Rev. C **92**, 044331 (2015).
[39] R. D. Lawson, *Theory of the Nuclear Shell Model* (Clarendon, Oxford, 1980), p. 184.